AFRL-AFOSR-UK-TR-2019-0062

Nonlinear quantum plasmonics: a quantum hydrodynamic approach

Cristian Ciraci
FONDAZIONE ISTITUTO ITALIANO DI TECNOLOGIA
VIA MOREGO 30
GENOVA, 16163
IT

11/25/2019
Final Report

Air Force Research Laboratory
Air Force Office of Scientific Research
European Office of Aerospace Research and Development
Unit 4515 Box 14, APO AE 09421

REPORT DOCUMENTATION PAGE

Form Approved
OMB No. 0704-0188

1. REPORT DATE *(DD-MM-YYYY)*	2. REPORT TYPE	3. DATES COVERED *(From - To)*
25-11-2019	Final	01 Mar 2017 to 28 Feb 2019

4. TITLE AND SUBTITLE
Nonlinear quantum plasmonics: a quantum hydrodynamic approach

5a. CONTRACT NUMBER

5b. GRANT NUMBER
FA9550-17-1-0177

5c. PROGRAM ELEMENT NUMBER
61102F

6. AUTHOR(S)
Cristian Ciraci

5d. PROJECT NUMBER

5e. TASK NUMBER

5f. WORK UNIT NUMBER

7. PERFORMING ORGANIZATION NAME(S) AND ADDRESS(ES)
FONDAZIONE ISTITUTO ITALIANO DI TECNOLOGIA
VIA MOREGO 30
GENOVA, 16163 IT

8. PERFORMING ORGANIZATION REPORT NUMBER

9. SPONSORING/MONITORING AGENCY NAME(S) AND ADDRESS(ES)
EOARD
Unit 4515
APO AE 09421-4515

10. SPONSOR/MONITOR'S ACRONYM(S)
AFRL/AFOSR IOE

11. SPONSOR/MONITOR'S REPORT NUMBER(S)
AFRL-AFOSR-UK-TR-2019-0062

12. DISTRIBUTION/AVAILABILITY STATEMENT
A DISTRIBUTION UNLIMITED: PB Public Release

13. SUPPLEMENTARY NOTES

14. ABSTRACT
In this project we have developed a new theoretical model for the nonlinear electrodynamic response at metal surfaces and obtained a numerical implementation of such model suitable for arbitrarily shaped geometries. Our approach is based on the quantum hydrodynamic theory (QHT), which allows to include spatially dependent electron density profiles in order to account for spill-out effects at the boundaries of a metallic system. The accuracy of the QHT however is based on the energy functionals used to describe the free-electron gas internal energy. We have developed a numerical implementation for multishell structures and compared QHT results to time-dependent density functional theory (TDDFT) calculations for systems in which quantum tunneling or quantum size effects could not be neglected. The generality of the QHT approach allowed also to consider nonlinear dynamics of free electrons. We have expanded for the first time the QHT equations beyond the linear approximation and performed second-harmonic generation (SHG) calculations for metallic slabs (and cylinders) and compared the QHT results to experimentally measured efficiencies. Moreover, we have investigated the spectral dependence of the SHG process and found resonances induced by the spill-out of the electron density at the metal surface that could in principle increase the SHG efficiency by several order of magnitude.

15. SUBJECT TERMS
EOARD, Plasmonic, Nonlinear optics, Nonlinear optical interactions, Optoelectronics, Quantum surface effects, Quantum hydrodynamic theory

16. SECURITY CLASSIFICATION OF:			17. LIMITATION OF ABSTRACT	18. NUMBER OF PAGES	19a. NAME OF RESPONSIBLE PERSON
a. REPORT	b. ABSTRACT	c. THIS PAGE			FOLEY, JASON
Unclassified	Unclassified	Unclassified	SAR		19b. TELEPHONE NUMBER *(Include area code)* 011-44-1895-616036

Standard Form 298 (Rev. 8/98)
Prescribed by ANSI Std. Z39.18

Technical Report

Grant #: FA9550-17-1-017

Project title:

Nonlinear quantum plasmonics: a quantum hydrodynamic approach

Abstract

In this project we have developed a new theoretical model for the nonlinear electrodynamic response at metal surfaces and obtained a numerical implementation of such model suitable for arbitrarily shaped geometries. Our approach is based on the quantum hydrodynamic theory (QHT), which allows to include spatially dependent electron density profiles in order to account for spill-out effects at the boundaries of a metallic system.
The accuracy of the QHT however is based on the energy functionals used to describe the free-electron gas internal energy. We have developed a numerical implementation for multi-shell structures and compared QHT results to time-dependent density functional theory (TD-DFT) calculations for systems in which quantum tunneling or quantum size effects could not be neglected.
The generality of the QHT approach allowed also to consider nonlinear dynamics of free-electrons. We have expanded for the first time the QHT equations beyond the linear approximation and performed second-harmonic generation (SHG) calculations for metallic slabs (and cylinders) and compared the QHT results to experimentally measured efficiencies. Moreover, we have investigated the spectral dependence of the SHG process and found resonances induced by the spill-out of the electron density at the metal surface that could in principle increase the SHG efficiency by several order of magnitude.

Keywords: plasmons; nonlocal effects; hydrodynamic model; smooth density profile; spatial dispersion; quantum hydrodynamic theory; second-harmonic generation; nonlinear dynamics; orbital-free.

INTRODUCTION

Quantum interactions in deeply confined light modes – plasmonic gap modes – might enable novel and efficient nonlinear processes. The possibility of designing quantum nonlinear properties presents several conceptual and technical challenges: *i)* numerical engineering of the hyperpolarizability via quantum surface effect, and *ii)* design of the systems able to couple the far-field into nanoscale-structured volumes.

In order to overcome these challenges, in this project we have developed a new theoretical model for the nonlinear electrodynamic response at metal surfaces and obtained a numerical implementation of such model suitable for arbitrarily shaped geometries. Our approach was based on the orbital-free quantum hydrodynamic theory (QHT). At the basis of the QHT is the following equation for the electron dynamics [1]:

$$\frac{\partial \mathbf{J}}{\partial t}+\gamma \mathbf{J}=\frac{e^2 n}{m_e}\mathbf{E}+\frac{en}{m_e}\nabla\frac{\delta G}{\delta n}+\frac{e}{m}\nabla\cdot\sigma-\frac{e}{m_e}\mathbf{J}\times\mathbf{B}+\frac{1}{e}\left(\frac{\mathbf{J}}{n}\nabla\cdot\mathbf{J}+\mathbf{J}\cdot\nabla\frac{\mathbf{J}}{n}\right) \qquad (1)$$

where the electron density $n(\mathbf{r})$ and the electron current $\mathbf{J}(\mathbf{r})$ are related through the continuity equation $\partial n/\partial t=\nabla\cdot\mathbf{J}/e$, m_e and e, the electron mass and the electron charge (in absolute value) respectively, and γ the phenomenological damping rate; $G[n] = T_{TF}[n] + 1/\eta T_{vW}[n, \nabla n] + E_{XC}[n]$ is the electron gas total internal energy, which in general includes the Thomas-Fermi (T_{TF}) and von Weizsäcker (T_{vW}) kinetic terms and exchange-correlation energy term (E_{XC}). σ is a viscoelastic-like tensor and takes into account the nonlocal damping [2]. The QHT equation is solved with Maxwell's equations for the electromagnetic fields **E** and **B**.

The accuracy of the QHT relies then on the specific energy functional $G[n]$ that is used. The most important contribution in $G[n]$ is given by the non-interacting kinetic energy. In its simplest approximation, $G[n]$ depends only on the electron density n (*Thomas-Fermi* (TF) theory [3]). In general $G[n]$ introduces an electron pressure term that prevents the induced electron density to collapse into a null volume and it rather spreads out from the surface into the bulk region [4], in contradistinction to the local response approximation, where induced charges are crushed into an infinitesimally thin layer at the surface of the metal. $G[n]$ can be further improved by considering terms depending (in general nonlinearly) on ∇n, $\nabla^2 n$, and so on.

In order to study the accuracy of the QHT it is useful to compare QHT results against more traditional models, such as the local response approximations (LRA) and the Thomas-Fermi Hydrodynamic theory (TF-HT), and against full quantum calculations obtained using time-depended density functional theory (TD-DFT). The main differences of these models are outlined in Fig. 1 [5].

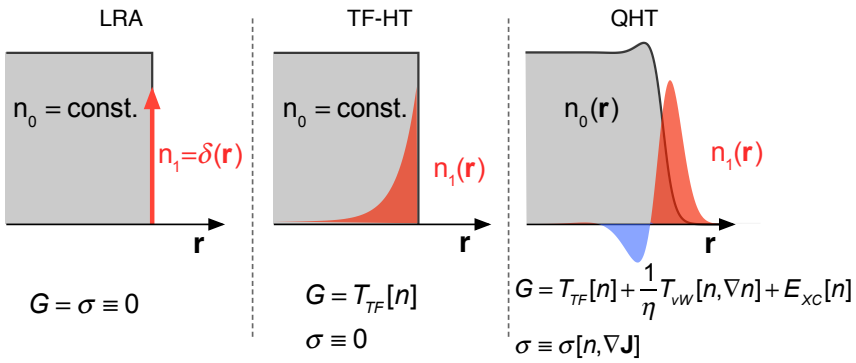

Figure 1: Summary of the three different response models. In the LRA, the induced charge density is a Dirac delta function centered at the metal surface; in the TF-HT, electrons accumulate near the metal surface without being able to escape; in the QHT the equilibrium density is exponentially decaying across the metal surface and the induced charges are smeared both in and out the metal-air interface.

RESULTS

The main results obtained under the support of this grant are summarized in this section. We have divided our results into two sub-sections: *published work*, for the work that can be referred to publications written with support of this grant, and *unpublished work,* for the work that has not yet been published.

Published work

The key element of the project is obtaining an energy functional $G[n]$ that accurately describes the free-electron dynamics. Although many functional have been developed in the context of orbital-free methods [6, 7], few of these functionals have been applied for the linear response of plasmonic structures, and virtually none has been applied in the sub-nanometer gap regime, where nonlocal and quantum effects are most important.

It is very important then to study the behavior of these functionals in these extreme systems, in order to assess their suitability for predicting nonlinear optical effects. For this reason, we have tested state-of-the art functionals in sub-nanometer gap nested shells (nano-matryoshka) plasmonic systems. This system is shown in Fig. 2. Its spherical symmetry makes it possible to perform calculation with TD-DFT, which is notoriously computational very demanding.

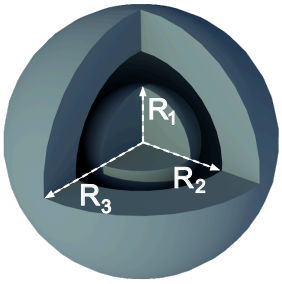

Figure 2: Geometry of the nano-matryoshka (NM) structure made up of a solid metallic core encapsulated by a concentric metallic shell. In this document we will consider NMs with sizes ($R1$, R_2, R_3) = SF × (8.5, 9.5, 15.9) Å, SF being a scaling factor.

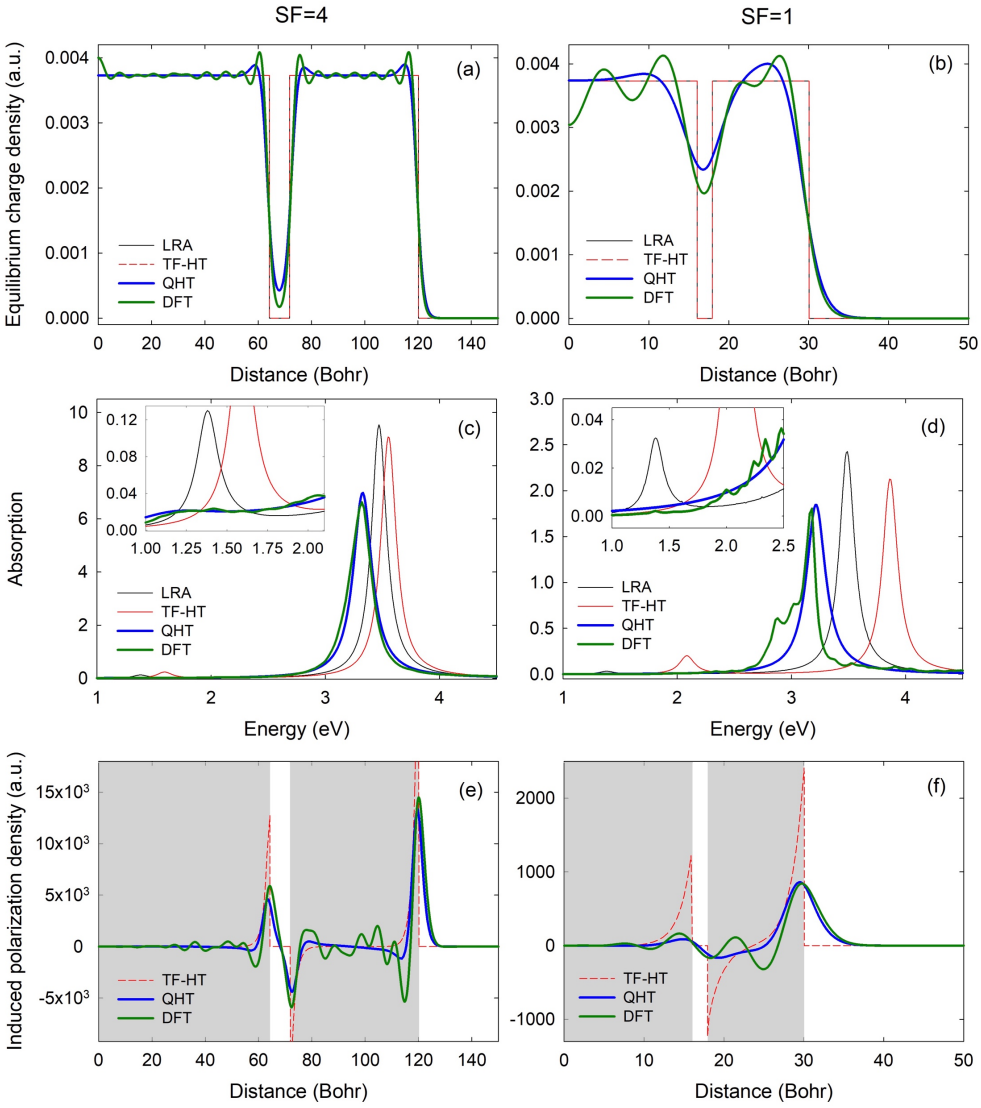

Figure 3: (a,b) Ground-state density, (c,d) absorption efficiency, and (e,f) induced polarization density obtained as $n_{\text{ind}} = \nabla \cdot \mathbf{P}/e$ for SF=4 (left panels) and SF=1 (right panels) for LRA,TF-HF, QHT and TD-DFT calculations.

The QHT model in the linear response reduces to the following set of coupled equations:

$$\nabla \varepsilon_\infty \nabla \frac{\delta G}{\delta n}\bigg|_{n=n_0} + \frac{e^2}{\varepsilon_0}\left(n_0 - n^+\right) = 0 \tag{2}$$

$$\nabla \times \nabla \times \mathbf{E} - \frac{\omega^2}{c^2} = \mu_0 \omega^2 \mathbf{P} \tag{3}$$

$$\frac{en_0}{m_e} \nabla \frac{\delta G^{(1)}}{\delta n} + \frac{e}{m} \nabla \cdot \sigma^{(1)} - \left(\omega^2 + i\omega\gamma\right)\mathbf{P} = \frac{e^2 n_0}{m_e}\mathbf{E} \tag{4}$$

Eq. (2) being the equation for the self-consistent equilibrium density n_0, while the Eqs. (3) and (4) describe the electromagnetic linear response. The superscript (1) indicate the linear order dependence in $n_1 = \nabla \cdot \mathbf{P}/e$.

We have implemented the previous equations in Comsol Multiphysics [8], a commercially available software that allows for a flexible implementation of arbitrary equations. We exploit the symmetry of the geometry and use the 2.5D simulation technique [9], which significantly reduces the computational efforts in terms of memory and processing time. 2.5D method requires all fields to be written in terms of an azimuthal mode number m, such that for a vector field $\mathbf{v}$ can be expressed as: $\mathbf{v}(\rho, \phi, z) = \Sigma_m \mathbf{v}^{(m)}(\rho, z) \exp[-im\phi]$, where $m \in Z$. The advantage of this method is that an initially three-dimensional problem is reduced to a few $(2m_{max} + 1)$ two-dimensional problems. For sub-wavelength structures $m_{max} < 3$ is usually enough to accurately describe the problem.

We solve Eqs. (2)-(4) for nested shells (nano-matryoshka) to calculate their QHT linear response and compare our results against LRA, TF-HT and TD-DFT results. By varying the distance between two concentric shells it is possible to study different overlapping regimes of the electron density tails.

We summarize our main results in Fig. 3, where we report (from top to bottom) the ground-state density n_0, the linear absorption spectrum, the induced charge density n_1 at the resonance peak, for SF = 4, 1 (see caption in Fig. 2).

The QHT approach reproduces very accurately the main features of the TD-DFT results, including the oscillations at the external surface of the system as well as inside the gap. Interestingly, also QHT field enhancement results are in good agreement with TD–DFT, as shown in Fig. 4 as a function of the system (gap) size [10].

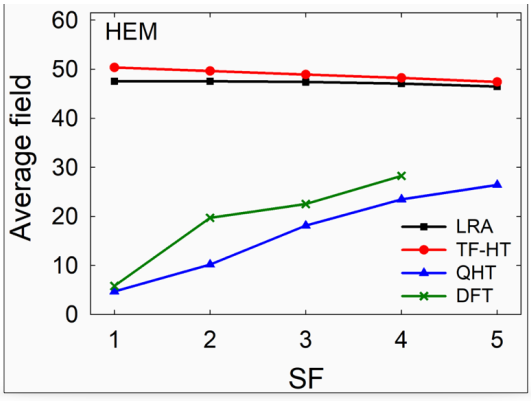

Figure 4: Average electric field enhancement inside the gap as a function of scaling factor (SF) for Na NMs at HEM computed using LRA, TF–HT, QHT and TD-DFT methods.

Furthermore, we have used the QHT to investigate the impact of nonlocality and electron spill-out on the plasmonic behavior of spherical Na and Au nanoshells. We adopted a self-consistent way to compute the equilibrium charge density. The results predicted by QHT were compared with those obtained with LRA and TF-HT. We found that nonlocal effects have a strong impact on both the near- and far-field optical properties of nanoshells, in particular, for the antibonding resonant mode, as shown in Fig. 4. We also investigated the optical

response of these systems for different thicknesses of the shell, both for Na and Au metals [11].

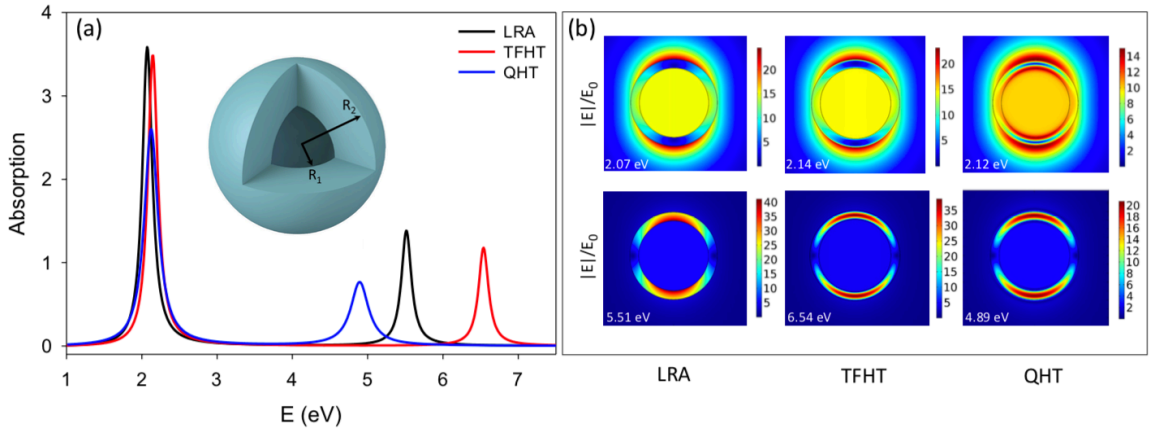

Figure 5: (**a**) Absorption efficiency of Na nanoshell with *R*1 = 2 nm and *R*2 = 2.5 nm calculated using local response approximation (LRA), Thomas–Fermi hydrodynamic theory (TFHT), and quantum hydrodynamic theory (QHT). (**b**) Electric field distribution plotted at corresponding resonance frequencies, both at lower (upper panel) and higher energy modes (lower panel), computed using different methods.

The results of this section have been published and presented in the following articles and conferences:

- M. Khalid and C. Ciracì, "*Numerical Analysis of Nonlocal Optical Response of Metallic Nanoshells*", Photonics **6**, 39 (2019);
- M. Khalid, F. Della Sala, and C. Ciracì, "*Optical properties of plasmonic core-shell nanomatryoshkas: a quantum hydrodynamic analysis*", Opt. Express **26**, 17322 (2018);
- M. Khalid and C. Ciracì, (2019) "*Impact of nonlocality, electron spill-out and tunneling on optical properties of metallic nanoshell and core-shell structures*". Oral presentation at " Quantum Nanophotonics", March 17-23, Benasque, SPAIN;
- C. Ciracì and M. Khalid, F. Della Sala, (2018) "*Optical properties of core-shell systems with sub nanometer plasmonic gaps: a quantum hydrodynamic theory approach*". Oral presentation at "Metamaterials' 2018", August 27-30, Espoo, FINLAND;
- M. Khalid and C. Ciracì, (2018) "*Analysis of Spherical Core-Shell Structures with Sub-nanometer Plasmonic Gaps*". Oral presentation at " Plasmonica 2018", July 4-6, Florence, ITALY;
- M. Khalid and C. Ciracì, (2018) "*Numerical study of spherical nanomatryoshkas by using quantum hydrodynamic theory*". Oral presentation at "SPIE NanoScience + Engineering", August 19-23, San Diego CA, USA;
- C. Ciracì, (2017) "*Quantum Hydrodynamic Theory for nonlinear optical applications*". Invited presentation at "META 2017", July 25-28, Seoul, SOUTH KOREA;

Unpublished results

The evaluation of the goodness in the linear regime of the functional used was a crucial step in order to obtain a QHT that is valid for the nonlinear dynamics. Here we go beyond the linear approximation and consider terms up to the second order. This allows to study second-harmonic generation (SHG) from metal surfaces. In order to simplify our calculations, we assume that the fundamental field is not perturbed by the conversion process (undepleted pump approximation). Assuming that the field can be written as a sum of harmonic contributions at ω_1 and $\omega_2 = 2\omega_1$, i.e. $\mathbf{E}(\mathbf{r},t) = \mathbf{E}_1(\mathbf{r})e^{-i\omega_1 t} + \mathbf{E}_2(\mathbf{r})e^{-i\omega_2 t} + \text{c.c.}$ **,** from Eq. (1) we obtain the following system of equations for the polarization vector **P** = **J**/iω:

$$\begin{aligned} -\frac{en_0}{m}\nabla\left(\frac{\delta G[n]}{\delta n}\right)_1 - \frac{i\omega_1}{m}\nabla\cdot\sigma_1 - \left(\omega_1^2 + i\gamma\omega_1\right)\mathbf{P}_1 &= \frac{e^2 n_0}{m}\mathbf{E}_1, \\ -\frac{en_0}{m}\nabla\left(\frac{\delta G[n]}{\delta n}\right)_2 - \frac{i\omega_2}{m}\nabla\cdot\sigma_2 - \left(\omega_2^2 + i\gamma\omega_2\right)\mathbf{P}_2 &= \frac{e^2 n_0}{m}\mathbf{E}_2 + \mathbf{S}_{\text{NL}}, \end{aligned} \tag{5}$$

Where the nonlinear source term is:

$$\begin{aligned} \mathbf{S}_{\text{NL}} = \frac{e^2 n_1}{m}\mathbf{E}_1 - \frac{\omega_1^2}{en_0}\mathbf{P}_1\nabla\cdot\mathbf{P}_1 - \frac{\omega_1^2}{e}\mathbf{P}_1\cdot\nabla\frac{\mathbf{P}_1}{n_0} + i\omega_1\frac{\mu_0 e}{m}\mathbf{P}_1\times\mathbf{H}_1 + \\ + \frac{en_1}{m}\nabla\left(\frac{\delta G[n]}{\delta n}\right)_1 + \frac{en_0}{m}\nabla\left(\frac{\delta G[n]}{\delta n}\right)_2^{(\text{NL})} + \frac{i\omega_2}{m}\nabla\cdot\sigma^{(2)} \end{aligned} \tag{6}$$

Explicit expressions for each of the terms in the second row of Eq. (6) are quite complex and are reported in the Appendix at the end of the document. It is important to know that the von Weizsäcker term in G[n] is usually weighted by a factor $1/\eta$, where $1 \le \eta \le 9$. In what follow we will use distinct parameter for the linear (η_L) and nonlinear (η_{NL}) contributions.

Eqs. (5) and (6) together with Maxwell's equations can be used to calculate SHG from a metal surface as a function of the incidence angle as sketched in the left panel of Fig. 6. In particular we apply the nonlinear QHT to investigate the SHG from an Ag film. It is important to remark that optical behavior of a plasmonic system is a sensitive function of ground-state electron density profile. Hydrodynamic model in the TF approximation does not give reliable results for the realistic ground-state density profiles [12]. The QHT method, on the other hand, is able to deal with the realistic profiles in a remarkably efficient way, as it has been reported in the first part of this report. We compute the ground-state charge density for Ag slab self-consistently by using Eq. (2) for different values of core-permittivity ε_∞ as shown in the right panel of Fig. 6. $\varepsilon_\infty = 1$ is the case when the contribution due to core charges is neglected. 'E' in the legends refers to the situation when 1 Å distance between the edge of the positive background and the first plane of the nuclei is considered. We input this density to our system of nonlinear QHT Eqs. (5) and (6) to study the SHG from a thick Ag slab as a function of the incident angle for a TM polarized pump tuned at λ = 1064 nm.

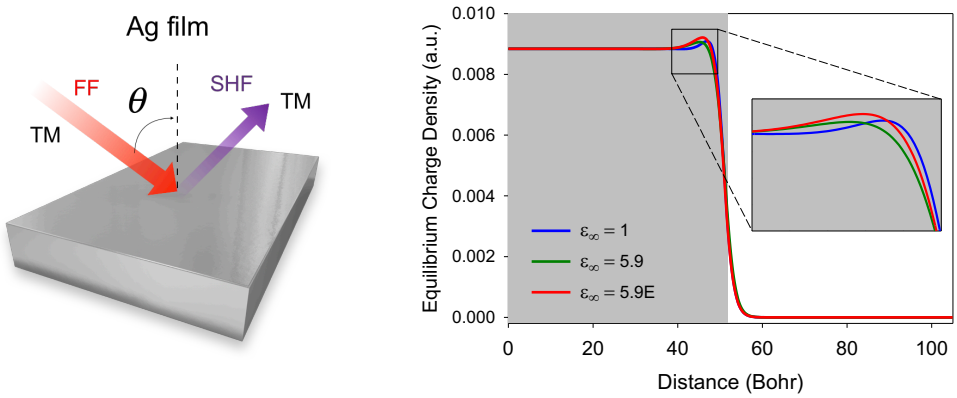

Figure 6: (Left) SHG numerical setup. (Right) Equilibrium charge density for different values of core-permittivity (ε_∞) computed self-consistently. Inset shows a zoom in on the quantum oscillation near the metal interface and the shaded grey region represents the metal.

SHG efficiency plotted as a function of angle for different input ground-state densities is given in Fig. 7 and the results are compared with the experimental data [13]. Here we present results for $\eta_{NL} = 1$ (left) and $\eta_{NL} = 9$ (right) whereas $\eta_L = 1$ for both cases. It can be seen from the results that for $\eta_{NL} = 1$, $\varepsilon_\infty = 1$ approximates quantitatively the experimental data, although the angle dependence is not well reproduced. However, if we consider $\eta_{NL} = 9$ it underestimates the SHG efficiency, nevertheless the angle dependence agrees very well qualitatively with the experimental data especially when contribution due to background charges is considered.

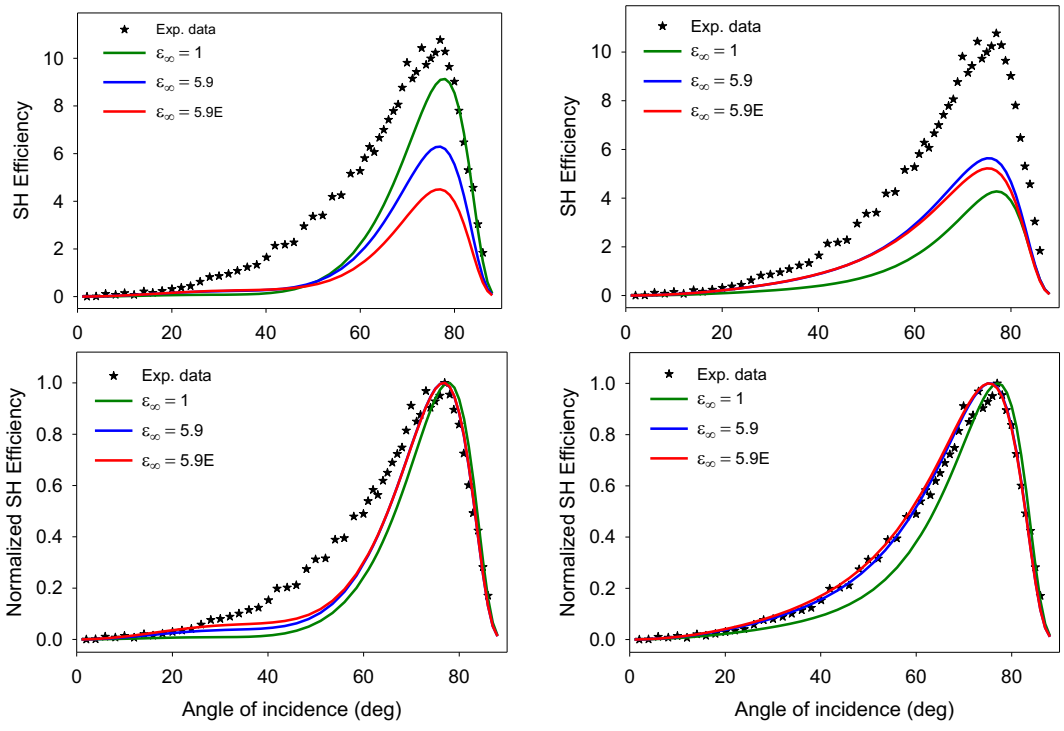

Figure 7: SHG efficiency as a function of angle of incidence for different cases of the background core permittivity ε_∞. 'E' in the legends refers to the case when 1 Å distance between the edge of the positive background and the first plane of the nuclei is considered. Left panel presents the results for $\eta_{NL} = 1$ and right panel for $\eta_{NL} = 9$. Lower panel shows the spectra normalized with respect to the maximum value of the SHG efficiency.

We now analyze the nonlinear response of the Ag film as a function of the pump frequency. SHG efficiency spectra for a fixed incident angle θ are plotted in Fig. 8 for different values of $\eta_L = \eta_{NL} = \eta$.

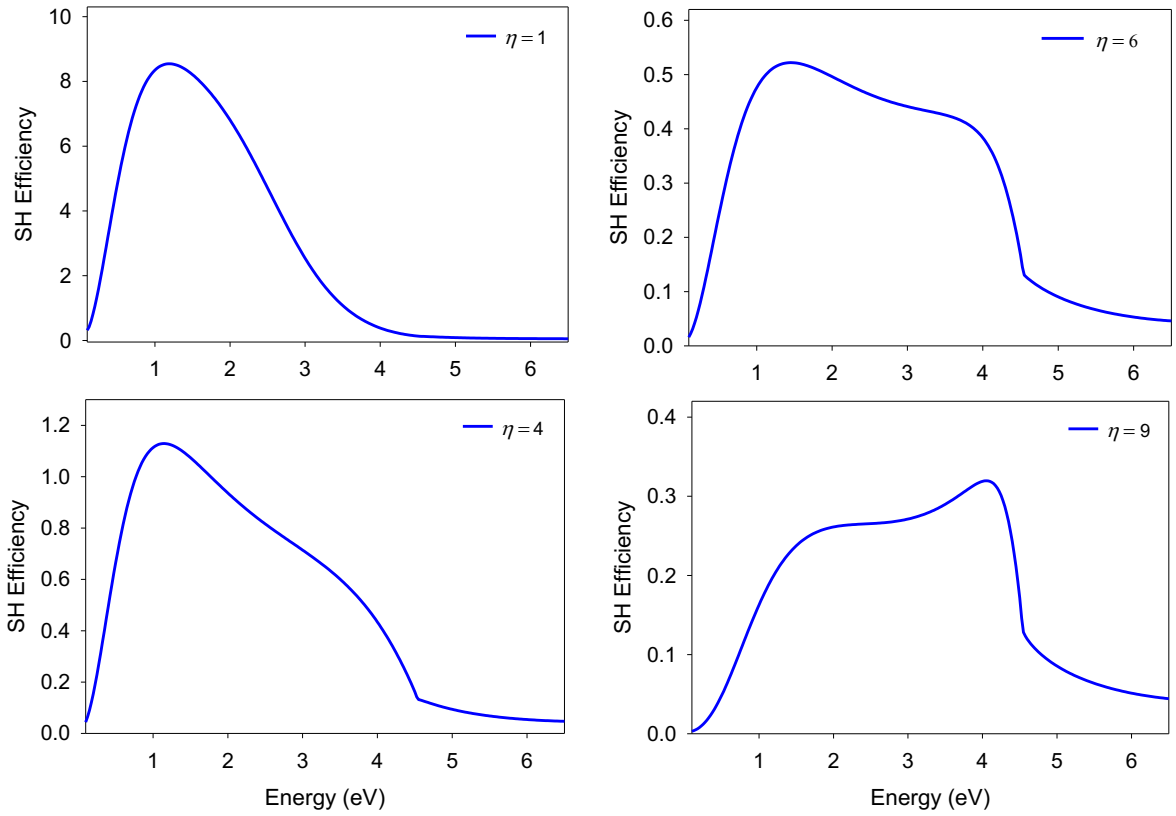

Figure 8: SHG efficiency as function of fundamental energy for a TM polarized plane wave impinging at an angle $\theta = 75°$ with respect to the surface normal.

We observe that the SHG efficiency shows some structures in the spectra for each η, although quite broader. In the following, we neglect the viscoelastic tensor which takes into account the broadening of the plasmon resonances and for simplicity we also ignore the contribution of background permittivity. We find that QHT predicts a neat and large resonance in the QHT spectrum as shown in Fig. 9. The results for different values of η are compared with the conventional TF-HT which does not display any structure since no electron spill-out effects are taken into account. We also report the SHG results for Ag infinitely long cylinder with circular cross-section and the spectra for different values of $\eta = \eta_L = \eta_{NL}$ show the same behavior as found in the case of film.

These resonances can be understood by looking at the linear reflectance shown in Fig. 10 computed within the QHT method for different value of η and compared against the TF-HT with hard-wall boundary conditions (no electron spill-out). The QHT method predicts a dip in the linear reflectance for each value of η. SH enhancement in the QHT nonlinear spectra presented in Fig. 9 can be associated to the dip in the linear spectra of the reflectance (Fig. 10) and which is a consequence of electron spill-out from the film surface into free-space. We do not see any resonance feature in the TFHT spectra due to the fact that it neglects the electron spill-out.

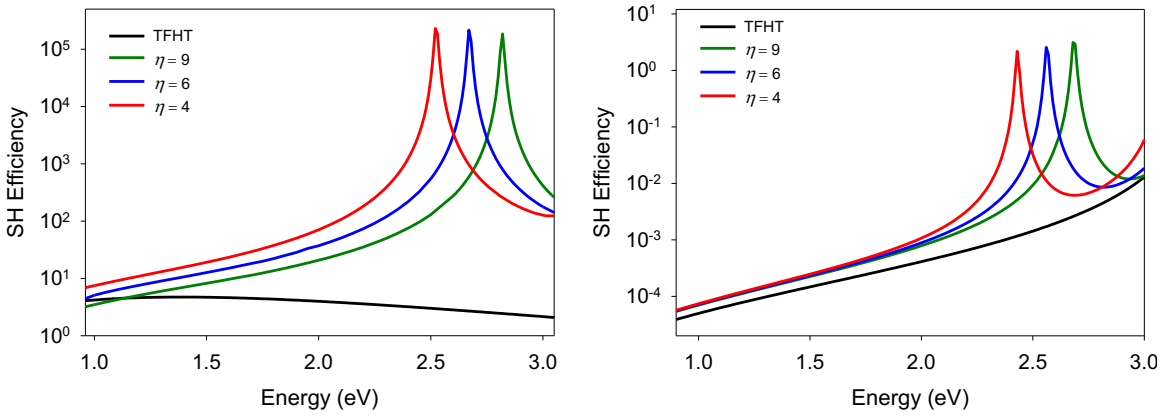

Figure 9: SHG efficiency as a function of fundamental energy. (Left) for the Ag slab shown in Fig. 6 with angle of incidence $\theta = 75°$; (Right) Ag infinite cylinder of 2 nm radius with circular cross-section.

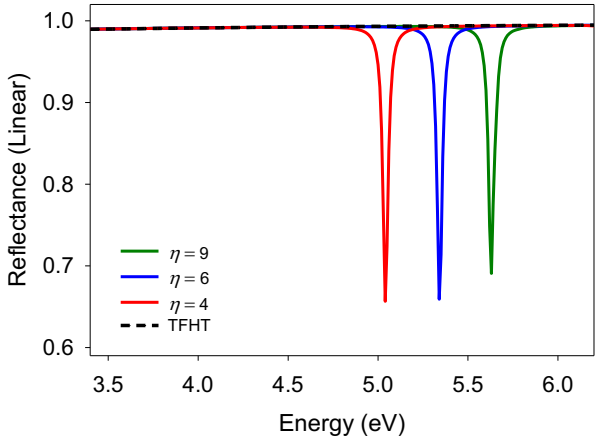

Figure 10: Linear reflectance from the Ag slab for different values of η calculated within the QHT method. The results are compared with the conventional TF-HT which overlooks the electron spill-out.

While conventional TF-HT is unable to deal with the realistic equilibrium charge density profiles as it yields spurious modes originating from the exponentially decaying tail of the electron density profile [14, 15], our QHT method works efficiently for the realistic ground-state densities giving rise to accurate predictions on the existence of surface resonances that can be exploited to generated more efficiently SH signals.

APPENDIX

The second-order contributions from the different energy components are:

$$\left(\frac{\delta T_{TF}}{\delta n}\right)_2^{\mathrm{NL}} = -\frac{5}{27} c_{TF} n_0^{-4/3} n_1^2,$$

$$\left(\frac{\delta T_{\mathrm{vW}}}{\delta n}\right)_2^{\mathrm{NL}} = \frac{\left|\nabla n_1\right|^2}{n_0^2} - 4\frac{\nabla n_0 \cdot \nabla n_1}{n_0^3} n_1 + 2\frac{\nabla^2 n_1}{n_0^2} n_1 + 3\frac{\left|\nabla n_0\right|^2}{n_0^4} n_1^2 - 2\frac{\nabla^2 n_0}{n_0^3} n_1^2,$$

and

$$\left(\frac{\delta E_{\mathrm{xc}}}{\delta n}\right)_2 = \frac{1}{2}\left(3\frac{d^2\varepsilon_{\mathrm{x}}}{dn^2} + n\frac{d^3\varepsilon_{\mathrm{x}}}{dn^3} + 3\frac{d^2\varepsilon_{\mathrm{c}}}{dn^2} + n\frac{d^3\varepsilon_{\mathrm{c}}}{dn^3}\right)_{n=n_0} n_1^2$$

where:

$$\frac{d^2\varepsilon_x}{dn^2} = \frac{2}{9} c_x n^{-5/3},$$

$$\frac{d^3\varepsilon_x}{dn^3} = -\frac{10}{27} c_x n^{-8/3},$$

$$\frac{d^2\varepsilon_c}{dn^2} = \begin{cases} \dfrac{1}{3}\left[\dfrac{r_s}{3}\left(5c + 4d + 4c\ln r_s\right) + a\right] n^{-2}, & r_s < 1 \\ -\dfrac{\gamma}{9}\left[\dfrac{\dfrac{7\beta_1}{4} r_s^{1/2} + 4\beta_2 r_s}{\left(1 + \beta_1 r_s^{1/2} + \beta_2 r_s\right)^2} + \dfrac{\left(\dfrac{\beta_1}{2} r_s^{1/2} + \beta_2 r_s\right)^2}{\left(1 + \beta_1 r_s^{1/2} + \beta_2 r_s\right)^4}\right] n^{-2}, & r_s \geq 1 \end{cases}$$

$$\frac{d^3\varepsilon_c}{dn^3} = \begin{cases} -\dfrac{1}{9}\left[\left(13c + \dfrac{28}{3}d + \dfrac{28}{3}c\ln r_s\right) r_s + 6a\right] n^{-3}, & r_s < 1 \\ \dfrac{\gamma}{9}\left[\dfrac{\dfrac{7\beta_1}{2} r_s^{1/2} + 8\beta_2 r_s}{\left(1 + \beta_1 r_s^{1/2} + \beta_2 r_s\right)^2} + \dfrac{\dfrac{7}{24}\beta_1 r_s^{1/2} + \dfrac{4}{3}\beta_2 r_s - \dfrac{7}{24}\beta_1^2 r_s - \dfrac{7}{8}\beta_1\beta_2 r_s^{3/2} - \dfrac{4}{3}\beta_2^2 r_s^2}{\left(1 + \beta_1 r_s^{1/2} + \beta_2 r_s\right)^3}\right. \\ \left. + \dfrac{2\left(\dfrac{\beta_1}{2} r_s^{1/2} + \beta_2 r_s\right)^2}{\left(1 + \beta_1 r_s^{1/2} + \beta_2 r_s\right)^4} - \dfrac{\left(\dfrac{\beta_1}{2} r_s^{1/2} + \beta_2 r_s\right)\left(-\dfrac{1}{6}\beta_1 r_s^{1/2} - \dfrac{2}{3}\beta_2 r_s + \dfrac{1}{6}\beta_1^2 r_s + \dfrac{1}{2}\beta_1\beta_2 r_s^{3/2} + \dfrac{2}{3}\beta_2^2 r_s^2\right)}{\left(1 + \beta_1 r_s^{1/2} + \beta_2 r_s\right)^5}\right] n^{-3}, & r_s \geq 1 \end{cases}$$

The second-order contribution from the viscosity term is:

$$\sigma_{\mu\nu}^{(2)} = -\tilde{\eta}^{(0)}\frac{n_1}{n_0^2}\left[\frac{\partial P_{1,\mu}}{\partial r_\nu}+\frac{\partial P_{1,\nu}}{\partial r_\mu}-\frac{2}{3}\delta_{\mu\nu}\nabla\cdot\mathbf{P}_1\right]+\tilde{\zeta}^{(0)}\frac{n_1}{n_0^2}\delta_{\mu\nu}\nabla\cdot\mathbf{P}+$$
$$-\tilde{\eta}^{(0)}\frac{1}{n_0^2}\left[P_\mu^{(1)}\left(\frac{\partial n_1}{\partial r_\nu}-\frac{2n_1}{n_0}\frac{\partial n_0}{\partial r_\nu}\right)+P_\nu^{(1)}\left(\frac{\partial n_1}{\partial r_\mu}-\frac{2n_1}{n_0}\frac{\partial n_0}{\partial r_\mu}\right)-\frac{2}{3}\delta_{\mu\nu}\mathbf{P}_1\cdot\left(\nabla n_1-\frac{2n_1}{n_0}\nabla n_0\right)\right]+$$
$$+\tilde{\zeta}^{(0)}\frac{1}{n_0^2}\delta_{\mu\nu}\mathbf{P}_1\cdot\left(\nabla n_1-\frac{2n_1}{n_0}\nabla n_0\right)$$
$$+\tilde{\eta}^{(1)}\left[\frac{\partial}{\partial r_\nu}\left(\frac{P_{1,\mu}}{n_0}\right)+\frac{\partial}{\partial r_\mu}\left(\frac{P_{1,\nu}}{n_0}\right)-\frac{2}{3}\delta_{\mu\nu}\nabla\cdot\left(\frac{\mathbf{P}_1}{n_0}\right)\right]+\tilde{\zeta}^{(1)}\delta_{\mu\nu}\nabla\cdot\left(\frac{\mathbf{P}_1}{n_0}\right)$$

Where the first-order coefficients expressed as a function of the Wigner-Seitz radius $r_s = \frac{1}{a_0}\left(\frac{3}{4\pi n_0}\right)^{1/3}$ are:

$$\eta^{(1)} = \hbar\frac{30r_s^{-3/2}+\frac{160}{3}r_s^{-1}-\frac{280}{9}r_s^{-2/3}+\frac{496}{9}r_s^{-1/3}}{\left(60r_s^{-3/2}+80r_s^{-1}-40r_s^{-2/3}+62r_s^{-1/3}\right)^2}n_1$$
$$K^{(1)} = (E_h)2n_0\left(\frac{d^2}{dn^2}\left[n\varepsilon_{xc}(n)\right]\right)_{n_0}+n_0^2\left(\frac{d^3}{dn^3}\left[n\varepsilon_{xc}(n)\right]\right)_{n_0}$$
$$\mu^{(1)} = E_h\left\{\frac{5a}{3}r_s^{-2}+\frac{4b}{3}r_s^{-1}+\frac{4}{3}\frac{(c-b)(r_s+15)}{(r_s+20)^2}\right\}n_1$$

References

[1] C. Ciracì, *Phys. Rev. B* **95**, 245434, 2017.
[2] G. Vignale and W. Kohn, *Phys. Rev. Lett.* **77**, 2037, 1996.
[3] S. Raza et al., *J. Phys. Condens. Matter* **27**, 183204, 2015.
[4] C. Ciracì *et al*., *ChemPhysChem* **14**, 1109, 2013.
[5] C. Ciracì and F. D. Sala, *Phys. Rev. B* **93**, 205405, 2016.
[6] A. Domps *et al.*, *Phys. Rev. Lett.* **80**, 5520, 1988.
[7] H. Xiang *et al., J. Phys. Chem. Lett*. **5**, 1163, 2014.
[8] COMSOL Multiphysics, http://www.comsol.com
[9] C. Ciracì *et al*., *Opt. Express* **21**, 9397-9406, 2013.
[10] M. Khalid *et al*., *Opt. Express* **26**, 17322, 2018.
[11] M. Khalid and C. Ciracì, *Photonics* 6, 39, 2019.
[12] J. A. Maytorena *et al*., *Phys. Rev. B* **51**, 2556, 1995.
[13] K. O'Donnell and R. Torre, *New J. Phys.* **7**, 154, 2005.
[14] N. D. Lang and W. Kohn, Phys. Rev. B 1, 4555, 1970.
[15] C. Schwartz and W. L. Schaich, *Phys. Rev. B* **26**, 7008, 1982.